Research Article | Vol. 25, No. 5 | 6 Mar 2017 | OPTICS EXPRESS 5480

Optics EXPRESS

Giant circular dichroism induced by tunable resonance in twisted Z-shaped nanostructure

YU QU, LISHUN HUANG, LI WANG, AND ZHONGYUE ZHANG*

School of Physics and Information Technology, Shaanxi Normal University, Xi'an 710062, China
**zyzhang@snnu.edu.cn*

Abstract: Circular dichroism (CD) is useful in molecular chemistry, pharmaceuticals, and bio-sensing. In this paper, twisted Z-shaped nanostructure (TZN) is proposed to achieve giant CD. The TZN is composed of three vertical and twisted nanorods. Given that the resonance of vertical nanorod is only observable for left circularly polarized light excitation but is subdued for right circularly polarized light excitation, which leads to the giant CD effect approaching 88%. The subdued resonance of vertical nanorod can be excited by rotating the bottom nanorod. The CD properties can be tuned by the length of nanorods and the gap between them. These results would guide the design of plasmonic chiral nanostructures for achieving giant CD effect.

OCIS codes: (260.2110) Electromagnetic optics; (240.6680) Surface plasmons; (160.1585) Chiral media; (250.5403) Plasmonics; (260.5740) Resonance.

References and links

1. S. M. Kelly, T. J. Jess, and N. C. Price, "How to study proteins by circular dichroism," Biochim. Biophys. Acta **1751**(2), 119–139 (2005).
2. M. Takezaki and Y. Kito, "Circular dichroism of rhodopsin and isorhodopsin," Nature **215**(5106), 1197–1199 (1967).
3. A. Kuzyk, R. Schreiber, Z. Fan, G. Pardatscher, E.-M. Roller, A. Högele, F. C. Simmel, A. O. Govorov, and T. Liedl, "DNA-based self-assembly of chiral plasmonic nanostructures with tailored optical response," Nature **483**(7389), 311–314 (2012).
4. E. Hendry, T. Carpy, J. Johnston, M. Popland, R. V. Mikhaylovskiy, A. J. Lapthorn, S. M. Kelly, L. D. Barron, N. Gadegaard, and M. Kadodwala, "Ultrasensitive detection and characterization of biomolecules using superchiral fields," Nat. Nanotechnol. **5**(11), 783–787 (2010).
5. W. Ma, H. Kuang, L. Xu, L. Ding, C. Xu, L. Wang, and N. A. Kotov, "Attomolar DNA detection with chiral nanorod assemblies," Nat. Commun. **4**(2689), 2689 (2013).
6. J. K. Gansel, M. Thiel, M. S. Rill, M. Decker, K. Bade, V. Saile, G. von Freymann, S. Linden, and M. Wegener, "Gold helix photonic metamaterial as broadband circular polarizer," Science **325**(5947), 1513–1515 (2009).
7. Y. Zhao, M. A. Belkin, and A. Alù, "Twisted optical metamaterials for planarized ultrathin broadband circular polarizers," Nat. Commun. **3**(870), 870 (2012).
8. Y. Yu, Z. Yang, S. Li, and M. Zhao, "Higher extinction ratio circular polarizers with hetero-structured double-helical metamaterials," Opt. Express **19**(11), 10886–10894 (2011).
9. J. B. Pendry, "A chiral route to negative refraction," Science **306**(5700), 1353–1355 (2004).
10. T. J. Davis and E. Hendry, "Superchiral electromagnetic fields created by surface plasmons in nonchiral metallic nanostructures," Phys. Rev. B **87**(8), 085405 (2013).
11. E. Plum, J. Zhou, J. Dong, V. A. Fedotov, T. Koschny, C. M. Soukoulis, and N. I. Zheludev, "Metamaterial with negative index due to chirality," Phys. Rev. B **79**(3), 035407 (2009).
12. M. Hentschel, L. Wu, M. Schäferling, P. Bai, E. P. Li, and H. Giessen, "Optical properties of chiral three-dimensional plasmonic oligomers at the onset of charge-transfer plasmons," ACS Nano **6**(11), 10355–10365 (2012).
13. C. Song, M. G. Blaber, G. Zhao, P. Zhang, H. C. Fry, G. C. Schatz, and N. L. Rosi, "Tailorable plasmonic circular dichroism properties of helical nanoparticle superstructures," Nano Lett. **13**(7), 3256–3261 (2013).
14. Y. He, G. K. Larsen, W. Ingram, and Y. Zhao, "Tunable three-dimensional helically stacked plasmonic layers on nanosphere monolayers," Nano Lett. **14**(4), 1976–1981 (2014).
15. Y. Wang, J. Deng, G. Wang, T. Fu, Y. Qu, and Z. Zhang, "Plasmonic chirality of L-shaped nanostructure composed of two slices with different thickness," Opt. Express **24**(3), 2307–2317 (2016).
16. J. Deng, J. Fu, J. Ng, and Z. Huang, "Tailorable chiroptical activity of metallic nanospiral arrays," Nanoscale **8**(8), 4504–4510 (2016).
17. J. Hu, X. Zhao, R. Li, A. Zhu, L. Chen, Y. Lin, B. Cao, X. Zhu, and C. Wang, "Broadband circularly polarizing dichroism with high efficient plasmonic helical surface," Opt. Express **24**(10), 11023–11032 (2016).

#279538 https://doi.org/10.1364/OE.25.005480
Journal © 2017 Received 26 Oct 2016; revised 4 Feb 2017; accepted 7 Feb 2017; published 1 Mar 2017

Optics EXPRESS

18. M. Kuwata-Gonokami, N. Saito, Y. Ino, M. Kauranen, K. Jefimovs, T. Vallius, J. Turunen, and Y. Svirko, "Giant optical activity in quasi-two-dimensional planar nanostructures," Phys. Rev. Lett. **95**(22), 227401 (2005).
19. W. X. Huang, Y. Zhang, X. M. Tang, L. S. Cai, J. W. Zhao, L. Zhou, Q. J. Wang, C. P. Huang, and Y. Y. Zhu, "Optical properties of a planar metamaterial with chiral symmetry breaking," Opt. Lett. **36**(17), 3359–3361 (2011).
20. F. Eftekhari and T. J. Davis, "Strong chiral optical response from planar arrays of subwavelength metallic structures supporting surface plasmon resonances," Phys. Rev. B **86**(7), 075428 (2012).
21. X. Lu, J. Wu, Q. Zhu, J. Zhao, Q. Wang, L. Zhan, and W. Ni, "Circular dichroism from single plasmonic nanostructures with extrinsic chirality," Nanoscale **6**(23), 14244–14253 (2014).
22. P. Zhang, M. Zhao, L. Wu, Z. Lu, Z. Xie, Y. Zheng, J. Duan, and Z. Yang, "Giant circular polarization conversion in layer-by-layer nonchiral metamaterial," J. Opt. Soc. Am. A **30**(9), 1714–1718 (2013).
23. X. R. Tian, Y. R. Fang, and B. Zhang, "Multipolar Fano resonances and Fano-assisted optical activity in silver nanorice heterodimers," ACS Photonics **1**(11), 1156–1164 (2014).
24. Y. Cui, L. Kang, S. Lan, S. Rodrigues, and W. Cai, "Giant chiral optical response from a twisted-arc metamaterial," Nano Lett. **14**(2), 1021–1025 (2014).
25. J. Dong, J. Zhou, T. Koschny, and C. Soukoulis, "Bi-layer cross chiral structure with strong optical activity and negative refractive index," Opt. Express **17**(16), 14172–14179 (2009).
26. M. Decker, R. Zhao, C. M. Soukoulis, S. Linden, and M. Wegener, "Twisted split-ring-resonator photonic metamaterial with huge optical activity," Opt. Lett. **35**(10), 1593–1595 (2010).
27. N. Liu, H. Liu, S. N. Zhu, and H. Giessen, "Stereometamaterials," Nat. Photonics **3**(3), 157–162 (2009).
28. X. Yin, M. Schäferling, B. Metzger, and H. Giessen, "Interpreting chiral nanophotonic spectra: the plasmonic Born-Kuhn model," Nano Lett. **13**(12), 6238–6243 (2013).
29. Y. Zhu, X. Y. Hu, Z. Chai, H. Yang, and Q. H. Gong, "Active control of chirality in nonlinear metamaterials," Appl. Phys. Lett. **106**(9), 091109 (2015).
30. B. Hopkins, A. N. Poddubny, A. E. Miroshnichenko, and Y. S. Kivshar, "Circular dichroism induced by Fano resonances in planar chiral oligomers," Laser Photonics Rev. **10**(1), 137–146 (2016).
31. S. Zu, Y. Bao, and Z. Fang, "Planar plasmonic chiral nanostructures," Nanoscale **8**(7), 3900–3905 (2016).
32. M. Schnell, P. Sarriugarte, T. Neuman, A. B. Khanikaev, G. Shvets, J. Aizpurua, and R. Hillenbrand, "Real-space mapping of the chiral near-field distributions in spiral antennas and planar metasurfaces," Nano Lett. **16**(1), 663–670 (2016).
33. A. B. Khanikaev, N. Arju, Z. Fan, D. Purtseladze, F. Lu, J. Lee, P. Sarriugarte, M. Schnell, R. Hillenbrand, M. A. Belkin, and G. Shvets, "Experimental demonstration of the microscopic origin of circular dichroism in two-dimensional metamaterials," Nat. Commun. **7**, 12045 (2016).
34. P. B. Johnson and R. W. Christy, "Optical constants of the noble metals," Phys. Rev. B **6**(12), 4370–4379 (1972).
35. B. Hopkins, A. N. Poddubny, A. E. Miroshnichenko, and Y. S. Kivshar, "Revisiting the physics of Fano resonances for nanoparticle oligomers," Phys. Rev. A **88**(5), 053819 (2013).
36. N. Verellen, Y. Sonnefraud, H. Sobhani, F. Hao, V. V. Moshchalkov, P. Van Dorpe, P. Nordlander, and S. A. Maier, "Fano resonances in individual coherent plasmonic nanocavities," Nano Lett. **9**(4), 1663–1667 (2009).

1. Introduction

Circular dichroism (CD) is the different absorption coefficient for left circularly polarized (LCP) and right circularly polarized (RCP) light by chiral objects. Chiral biomolecules naturally exhibit small CD signals that are difficult to detect in experiments [1–3]. Artificial chiral plasmonic nanostructures (ACPNs) exhibit larger CD than chiral biomolecules due to surface plasmonic resonance; ACPNs have been widely applied in biological monitoring [4, 5], circular polarizer [6–8], and negative refractive index media [9–11].

CD may arise from many different modes. 3D helix and helix-like ACPNs typically produce CD owing to the significant interactions between electric and magnetic resonance [12–17]. 2D planar ACPNs, such as gammadions, present relatively small CD resulted from the existence of only electric dipole mode [18, 19]. Some previous studies have considered oblique excitation for enhancing CD [20–23]. Under LCP and RCP excitations, large CD is generated because of the existence of electric and magnetic modes. Bi-layer twisted ACPNs, such as twisted-arc, bi-layer cross, and coupled-oscillator, exhibit larger chirality than single-layer ones, where bonding and anti-bonding modes exist [24–29]. Researchers in recent works have shown that plasmonic Fano resonance can enlarge the optical chirality by 30% in 2D planar metallic nanostructure. In these studies, CD signals appear at the same resonant modes for LCP and RCP excitations [30–33]. If CD signals are designed at different modes for LCP and RCP excitations, giant CD effect would occur.

Optics EXPRESS

In this paper, the twisted Z-shaped nanostructure (TZN) arrays are proposed and its optical properties are theoretically investigated by finite element method (FEM) simulations. The absorption spectra exhibit that an off-resonance dip for LCP and an anti-bonding resonance peak for RCP clearly occur at the same wavelength. As a result, a pronounced CD is generated with a maximum of 88%. The current density distributions demonstrate that the resonance of vertical nanorod is only excited for LCP but is subdued for RCP light. The effects of geometric parameters on CD are also studied. These findings can guide the design with strong optical chirality for practical application in bio-sensing.

2. Structure and computational method

The TZN in this study is composed of three mutually vertically displaced and twisted nanorods, as shown in Fig. 1(a). The front and top views with the definition of the associated parameters are displayed in Figs. 1(b) and 1(c). The top and bottom nanorods are in the same geometry parameters with fixed width of 30 nm and height of 30 nm, and varied lengths L. The vertical nanorod has fixed length of 30 nm and widths of 30 nm, and varied height H. G denotes the gap between the vertical nanorod and the top or bottom nanorods; θ expresses the rotary angle of the bottom nanorod with respect to x axis, $\theta = 90°$ in the TZN [Fig. 1(c)]. The TZN can be left- or right-handed depending on the rotary angle of the bottom nanorod. In this study, the periods of the TZN arrays are fixed with $P_x = 300$ nm and $P_y = 300$ nm in the x and y directions, respectively.

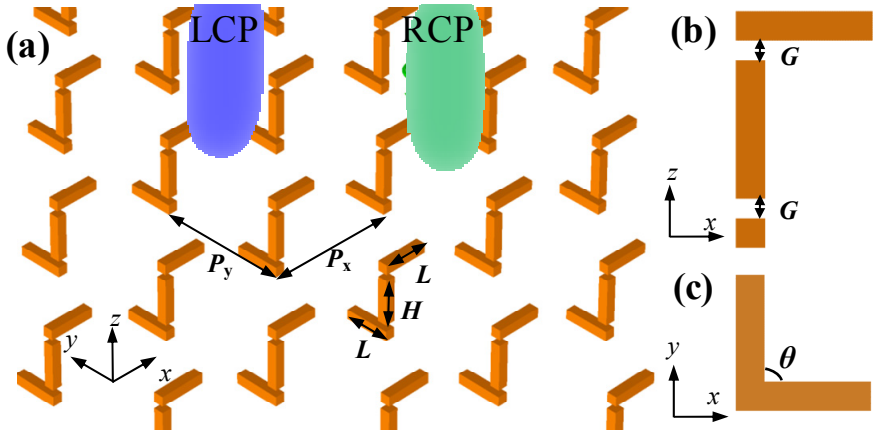

Fig. 1. Configuration of TZN arrays and parameters definition (a), where the unit cell with the associated geometric features are designated in (b) x-z plane and (c) x-y plane.

Three-dimensional finite element method software COMSOL Multiphysics is used to calculate the transmittance of the TZN arrays. The minimum mesh size (3 nm) is 10 times less than the minimum width (30 nm) of the TZN, which satisfies the COMSOL stability criteria (convergence). The refractive index of sliver is taken from Ref [34]. and the refractive index of air is fixed as 1. The excitation sources are RCP and LCP light along the -z direction and the magnitude of the incident electric field is set at 1 V/m. The infinite array is simulated using unit cell with periodic boundary conditions along the x and y directions. The Perfectly Matched Layers are applied at the top and bottom of the computational domain for absorbing light which pass through the Ports. The transmittance is defined as $T = P_{out} / P_{in}$, which is the ratio of output power to incident power. The absorption is defined as $A = 1\text{-}T\text{-}R$, where R is reflectivity. The optical chirality is defined as CD = $A_{LCP} - A_{RCP}$, where A_{LCP} and A_{RCP} is the absorption under LCP and RCP illumination.

Optics EXPRESS

3. Results and discussion

The absorption and CD spectra of structures with different parameters are calculated among the wavelengths from 0.5 μm to 1.0 μm. Figure 2(a) shows that the simulated absorption and CD spectra of the TZN arrays with $H = L = 140$ nm, $G = 20$ nm, and $\theta = 90°$. Under LCP illuminations (blue), two peaks of $\lambda = 0.65$ μm and $\lambda = 0.79$ μm and one broad dip region around $\lambda = 0.71$ μm are visibly observed. Under RCP illuminations (green), one narrow peak appears at $\lambda = 0.71$ μm. One narrow absorption peak occurs at $\lambda = 0.70$ μm for only horizontal nanorod; for the only vertical nanorod, the absorption is almost close to zero in the infrared region (not shown in this paper). At $\lambda = 0.71$ μm, the presence of dip and peak in the

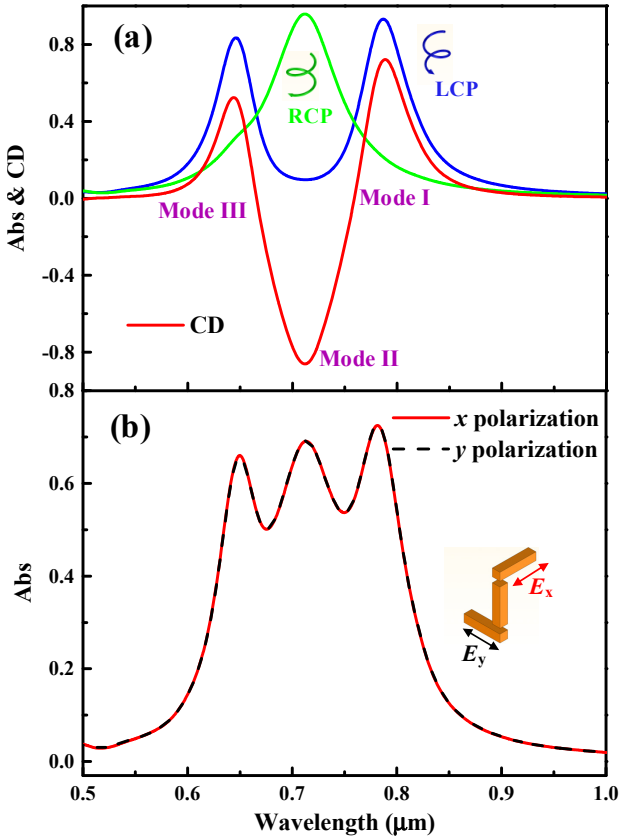

Fig. 2. The absorption and CD spectra of TZN arrays (a) under LCP and RCP illuminations; (b) under *x* and *y* polarization excitations.

absorption spectra of A_{LCP} and A_{RCP} leads to a significantly large CD of 88% (the red line in Fig. 2(a)). For simplicity, the resonance modes are divided into modes I, II, and III (labeled as Mode I, Mode II, and Mode III) in the CD spectrum. The CD spectra for right- and left-handed enantiomer are exactly mirror symmetric to each other. In order to investigate the associated physical dependencies of absorption spectra, the absorption of the TZN arrays under *x* and *y* polarization excitations are also studied [Fig. 2(b)]. Three peaks of $\lambda = 0.65$ μm, $\lambda = 0.71$ μm, and $\lambda = 0.78$ μm appear in the absorption spectrum. The absorption of the TZN arrays under *x* and *y* polarization excitation are overlap, which is resulted from the same parameters of top and bottom nanorods along *x* and *y* directions. Thus, the linear birefringence is negligible [26–28]. Given that a linearly polarized light consists of equivalent LCP and RCP light, the wavelength position of the absorption peaks for circular polarized light are coincident with that of linearly polarized light.

Optics EXPRESS

The modes of different peaks are emulated to understand the absorption mechanism of TZN arrays under linear polarization excitation. Figure 3(a) plots the proportional current densities at absorption peaks of the TZN for *x* polarization excitation. The red arrows denote the direction of current densities. The purple arrows in Fig. 3(b) represent the equivalent electric dipole moments of nanorods. At λ = 0.65 μm, the excited currents occur in the top and vertical nanorods, while the current in the bottom nanorod is relatively weak. As a result, effective electric dipole moments occur in the top and vertical nanorods. The courter-propagating electric dipoles of the top and vertical nanorods create bright anti-bonding mode [35, 36]. Correspondingly, at λ = 0.71 μm, the major current densities are distributed in the top and bottom nanorods and associated electric dipole moments form anti-bonding mode.

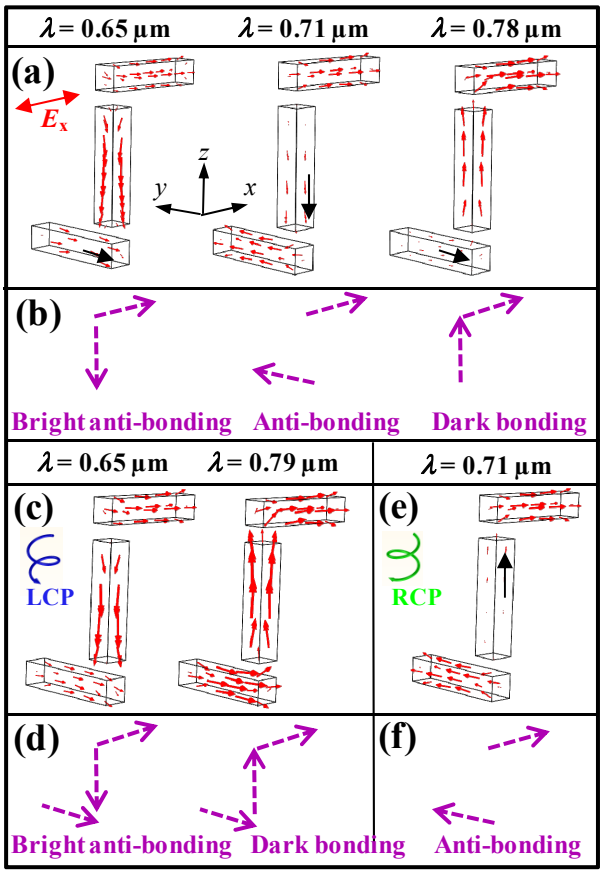

Fig. 3. The proportional current densities and the equivalent electric dipole moments at the absorption peaks for TZN under x polarizations excitation (a) and (b); under LCP excitation (c) and (d), and RCP excitation (e) and (f). The red arrows denote the direction of current densities; the black arrows reveal the direction of small current densities distributions; the purple arrows represent the equivalent electric dipole moments of nanorods.

Electric dipole mode occurs at λ = 0.70 μm for one horizontal nanorod structure (not shown in this paper). At λ = 0.78 μm, the intense currents in the top and vertical nanorods form an effective electric dipole, which is regarded as the dark bonding mode.

Using this argument, the proportional current densities and the equivalent electric dipole moments at the absorption peaks of the TZN for LCP and RCP excitations are also performed, as depicted in Figs. 3(c)–3(f). For LCP, the current densities of three nanorods reveal bright anti-bonding mode at λ = 0.65 μm and dark bonding mode at λ = 0.79 μm. The pronounced off-resonance dip at λ = 0.71 μm is due to the destructive interference between

Optics EXPRESS

the narrow bright mode and the broad dark mode. For RCP, at λ = 0.71 μm, the strong effective current densities are concentrated in the top and bottom nanorods. Accordingly, anti-bonding mode is induced. In the vertical nanorod the currents are negligible and the resonance is subdued; this phenomenon differs in LCP and RCP excitations. In other words, the effective charge oscillations in the vertical nanorod are polarization-controlled for circular polarized light, thereby resulting in the different dipoles coupled modes. The giant chirality in the absorption spectra emerges at the distinct resonance modes for LCP and RCP excitations. The chiral system of the TZN can be viewed as a right-handed enantiomer in which resonance is easier to be excited under LCP than under RCP illumination.

To explore the CD effects of TZN arrays for LCP and RCP excitations, rotary angle θ is changed from 0° to 90° with fixed $H = L$ = 140 nm, and G = 20 nm. Under RCP excitation, the subdued resonance in vertical nanorod is excited gradually as θ decreases [Fig. 4(a)]. Figure 4(b) illustrates that the amplitude of the three CD modes weaken distinctly, and the modes exhibit smooth spectrum shift with the decrease in θ. As θ = 0°, the TZN is achiral and the three modes disappear. The shift of Modes I and II is due to the change of the asymmetric resonance line shape. Therefore, rotating the bottom nanorod enables a way to switch on and off the resonance of TZN.

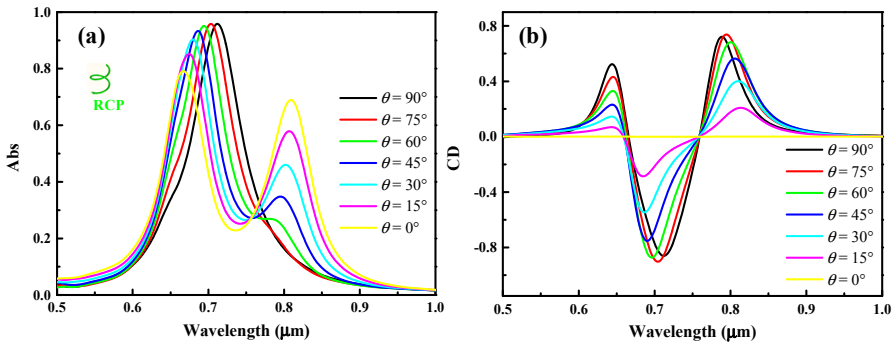

Fig. 4. The absorption and CD spectra of TZN arrays with varied θ values.

The spectra of varied parameters of TZN arrays are sequentially investigated to probe the mechanism of resonance in enhancing the CD effect. Gap G is first changed from 20 nm to 40 nm with fixed $H = L$ = 140 nm, and θ = 90° [Fig. 5(a)]. Modes I and II blue shifts, Mode III red shifts, and the magnitudes of CD signals decrease with the increase in G. Mode I is ascribed to the dark bonding mode for LCP, which presents the attraction between electric dipoles. As G increases, the attraction decreases, thereby leading to a decrease in the length of equivalent electric dipole oscillations and blue-shift of Mode I. On the contrary, Mode III is attributed to the bright anti-bonding mode showing repulsion between electric dipoles. An increase in G can decrease the repulsion, thus rendering the increased effective electric dipole moments and red-shift of Mode III. Mode II exhibits blue-shift because of the asymmetric narrowed resonance line shape with the increase in G. The increase in G causes the near-field coupling between the top or bottom nanorods and the vertical nanorod weakened. Accordingly, the resonance strength intensely weakens, thereby leading to the diminishing of CD signals. Figure 5(b) displays the CD spectra of H and L varying synchronously from 120 nm to 160 nm with fixed geometric parameters G = 20 nm and θ = 90°. Modes I, II, and III exhibit linearly red-shift with H and L increasing. This phenomenon is resulted from the extension of the effective electron oscillation length in three nanorods for LCP and RCP. Then the effect of the height of the vertical nanorod H on CD with fixed L = 140 nm, G = 20 nm, and θ = 90° is presented in Fig. 5(c). The obvious red-shifts of Modes I and III are due to the extended electric dipolar moment in resonance for LCP with the increase in H. Mode II originates from the anti-bonding mode of the top and bottom nanorods. The variation in H

Optics EXPRESS

slightly affects the shift of Mode II compared with the shifts of Modes I and III. Figure 5(d) reveals the influence of the variation in L on CD with fixed H = 140 nm, G = 20 nm, and θ = 90°. As L increases, the three modes all present obvious red shift by reason of the extended electric dipolar moments. In Figs. 5(c) and 5(d), the CD signals are maximal at the off-resonance dip as $H = L$ = 140 nm on account of matching resonant wavelength of nanorods. The value of H and L is relevant to the effective electron oscillation length in three nanorods. When $H = L$ = 140 nm, the wavelength of off-resonance dip for LCP matches that of anti-boding mode peak for RCP, then CD spectrum presents the highest value. In this paper, the period is fixed at P_x = 300 nm and P_y = 300 nm. With the further increase of the period, the resonant wavelengths exhibit red-shift (not shown in this paper).

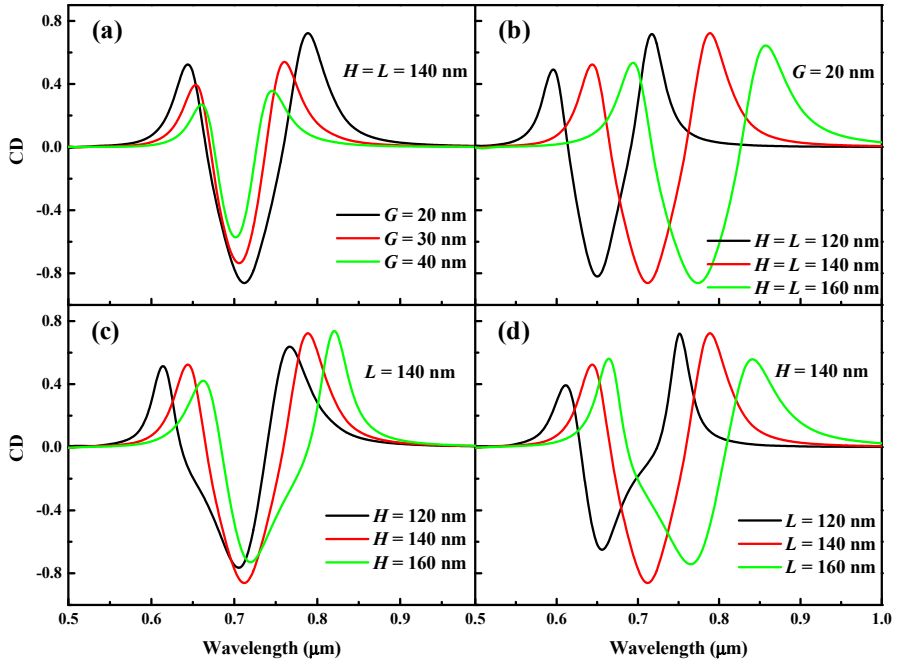

Fig. 5. The CD spectra of TZN arrays with (a) varied G values, (b) varied H and L values, (c) varied H values, and (d) varied L values.

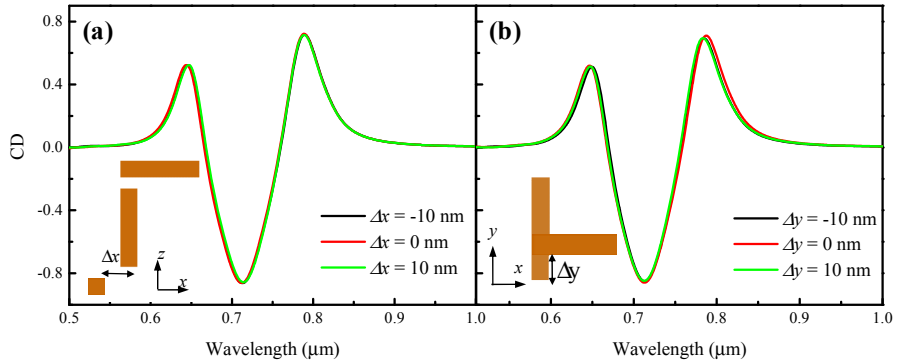

Fig. 6. The CD spectra of TNZ arrays with different displacements: (a) displacement of vertical nanorod Δx (the vertical nanorod and the top nanorod are well-aligned); (b) displacement of top nanorod Δy (the bottom nanorod and the vertical nanorod are well-aligned).

Optics EXPRESS

Experimentally, the TZN arrays can be fabricated through three runs of aligned electron beam lithography. The TZN is composed of three separated nanorods, so the displacement between nanorods layers along the x and y directions are inevitable during experimentation. To demonstrate the effect of the displacement, the CD spectra of different relative displacements are discussed, as shown in Fig. 6. Figure 6(a) reveals the displacement Δx between the vertical and bottom nanorod along the x direction (the top and vertical nanorod layers is well-aligned). Figure 6(b) illustrates the displacement Δy of top nanorod and vertical nanorod along the y direction (the bottom and vertical nanorod are well-aligned). Figure 6 show that the tiny displacement does not affect the CD properties obviously.

4. Conclusion

The TZN with three nanorods is proposed to produce giant CD of 88% at the distinct resonance modes. The TZN can be viewed as a right-handed enantiomer in which resonance is easier to be excited under LCP than under RCP illumination as a result of the polarization-controlled feature. The simulations reveal that the chirality in the absorption spectra is attributable to the different dipoles coupled modes of three nanorods for LCP and RCP due to the polarization-controlled characteristic in vertical nanorod. The subdued resonance of vertical nanorod under RCP can be excited by rotating the bottom nanorod, thereby resulting in the on and off switch of the resonance. Moreover, CD properties are intensely dependent on the length and gap of nanorods. These results can be helpful in understanding optical chirality induced by tunable resonance and can also guide the design of artificial chiral plasmonic nanostructures with large chirality.

Funding

National Natural Foundation of China (61575117); Fundamental Research Funds for the Central Universities of Ministry of Education of China (GK201601008); Innovation Funds of Graduate Programs, Shaanxi Normal University (2015CXS033); Fundamental Research Funds For the Central Universities (2016TS037).